Journal of Power Sources 193 (2009) 258–268

Contents lists available at ScienceDirect

Journal of Power Sources

journal homepage: www.elsevier.com/locate/jpowsour

Operational optimization and real-time control of fuel-cell systems

J. Hasikos, H. Sarimveis*, P.L. Zervas, N.C. Markatos

National Technical University of Athens, School of Chemical Engineering, 9 Heroon Polytechniou Str., GR-157 80 Athens, Greece

ARTICLE INFO

Article history:
Received 10 October 2008
Received in revised form 7 January 2009
Accepted 8 January 2009
Available online 29 January 2009

Keywords:
Fuel cells
Hydrogen
Model predictive control
Optimization
Meta-modeling
Neural networks

ABSTRACT

Fuel cells is a rapidly evolving technology with applications in many industries including transportation, and both portable and stationary power generation. The viability, efficiency and robustness of fuel-cell systems depend strongly on optimization and control of their operation. This paper presents the development of an integrated optimization and control tool for Proton Exchange Membrane Fuel-Cell (PEMFC) systems. Using a detailed simulation model, a database is generated first, which contains steady-state values of the manipulated and controlled variables over the full operational range of the fuel-cell system. In a second step, the database is utilized for producing Radial Basis Function (RBF) neural network "meta-models". In the third step, a Non-Linear Programming Problem (NLP) is formulated, that takes into account the constraints and limitations of the system and minimizes the consumption of hydrogen, for a given value of power demand. Based on the formulation and solution of the NLP problem, a look-up table is developed, containing the optimal values of the system variables for any possible value of power demand. In the last step, a Model Predictive Control (MPC) methodology is designed, for the optimal control of the system response to successive sep-point changes of power demand. The efficiency of the produced MPC system is illustrated through a number of simulations, which show that a successful dynamic closed-loop behaviour can be achieved, while at the same time the consumption of hydrogen is minimized.

1. Introduction

A fuel-cell system is a device where chemical energy from a fuel, such as hydrogen, is electrochemically converted to electrical and thermal energy, without combustion. Fuel cells operate at low noise levels and do not produce pollutant emissions. Fuel cells offer various economic and environmental advantages over internal-combustion engines and batteries. Due to those advantages, fuel-cell technology has come to the foreground for many mobile and terrestrial applications. In particular, the Proton Exchange Membrane Fuel-Cell (PEMFC) technology offers many advantages over other types of fuel cells (FCs); hence, this device has the potential to become a primary power source for power in the coming era.

However, the FC technology needs to tackle a variety of significant problems, in order to become more competitive and efficient compared to other energy technologies. In particular, fuel-cell systems pose many challenging problems as far as control and system integration are concerned, due to complicated system configurations and interactive subsystems, which lead to intricate transient dynamics and difficult control tasks.

In the literature, a number of control strategies and methodologies for fuel-cell systems have been proposed, that range from simple proportional–integral–derivative (PID) controllers to advanced control strategies such as fuzzy controllers and Model Predictive Control (MPC) methodologies.

Methekar et al. [1] considered a multi-input-multi-output (MIMO) system with inputs of hydrogen and coolant and outputs of power density and temperature, and proposed two PID control strategies. Woo and Benziger [2] demonstrated that the power output from a PEMFC can be directly regulated by limiting the hydrogen feed to the FC. Regulation was accomplished by varying the internal resistance of the membrane-electrode assembly in a self-draining FC with the effluents connected to water reservoirs.

Pukrushpan et al. [3] proposed both a feedforward controller and a Linear Quadratic Regulator (LQR) state feedback controller, for the online control of a PEMFC system. Guidong et al. [4] presented

Abbreviations: 3D, Three-Dimensional; CPU, Central Processor Unit; DC, Direct Current; FIR, finite impulse response; FC, fuel cell; LOO, Leave One-Out; LQG, Linear Quadratic Gaussian; LQR, Linear Quadratic Regulator; MIMO, multi-input-multi-output; MPC, Model Predictive Control; NLP, Non-Linear Programming; NNM, neural network model; PEMFC, Proton Exchange Membrane Fuel-Cell; PID, proportional–integral–derivative; PRESS, Prediction Error Sum of Squares; RBF, Radial Basis Function; RMSE, Root Mean Squared Error; SOFC, Solid Oxide Fuel Cell; SSE, Sum of Squared Errors between the observations and the predicted values; SSY, Sum of Squared Deviations between the observations and their mean.

* Corresponding author at: National Technical University of Athens, School of Chemical Engineering, Zografou University Campus, 15780 Athens, Greece. Tel.: +30 210 7723237; fax: +30 210 7723138.
E-mail address: hsarimv@chemeng.ntua.gr (H. Sarimveis).

0378-7753/$ – see front matter © 2009 Elsevier B.V. All rights reserved.
doi:10.1016/j.jpowsour.2009.01.048

Nomenclature

ch	control horizon
C	number of past inputs in the FIR model
$\mathbf{d}$	correction vector
f	Radial Basis Function
g_1, g_1	function symbols
h_i	ith coefficient in FIR model
$\mathbf{H}_i$	matrix containing the ith coefficients of a MIMO FIR model
I_{st}	stack current (A)
I^*_{st}	optimal value of stack current (A)
k	number of independent variables
L	number of hidden nodes in the neural network topology
M	number of output variables
n	number of the available data
N	number of input variables
ph	prediction horizon
P_D	power demand (W)
P_{net}	fuel-cell stack net power
$\mathbf{R}$	weight matrix
R^2	coefficient of determination (%)
R^2_{CV}	coefficient of determination by using the cross-validation technique (%)
T_i	sampling time (s)
$\mathbf{u}$	input vector
$\Delta\mathbf{u}$	vector of control moves
U_{cm}	compressor voltage (V)
U_{st}	stack voltage (V)
U^*_{cm}	optimal value of compressor voltage (V)
w_j	the weight corresponding to the response of the jth node in the neural network topology
$\mathbf{W}$	weight matrix
$\mathbf{x}$	input vector in the neural network model
$\mathbf{x}_j$	the centre of the jth node in the neural network topology
$\mathbf{y}$	output vector
$\hat{\mathbf{y}}$	prediction of output vector
$y_{m,i}$	true value of the mth output variable for the ith observation
$\hat{y}_{m,i}$	predicted value of the mth output variable for the ith observation
$\bar{y}_m$	mean of all values of the mth output variable over the available data set
$\hat{y}^{LOO}_{m,i}$	mth output variable prediction for observation i of the model that is trained using all the available data, except from observation i
$\mathbf{y}_{sp}$	set-point vector
z_j	The response of the jth node in the neural network topology

Greek symbols

λ_{O_2}	oxygen excess ratio
$\lambda^*_{\mathrm{O}_2}$	optimal value of oxygen excess ratio

a power management system, by employing a DC–DC module, a battery, a controller and some other circuits, as well as an LQR algorithm, which provided load with an approximately constant voltage, but also stabilized stack current by regulating charging or discharging current of the battery, according to the change of load. Rodatz et al. [5] designed a Linear Quadratic Gaussian (LQG) controller to decouple the pressure trace from the mass flow trace. Di Domenico et al. [6] extended this idea, by developing a multivariable LQG controller that is able to tune the excess air ratio while tracking the optimal pressurization to maximize system efficiency for transient loads.

Danzer et al. [7] proposed a multivariable flatness-based control technique, for controlling cathode pressure and oxygen excess ratio of a fuel cell, using the mass flow controller and the outlet throttle as actuators. Zenith and Skogestad [8] presented a method to control the output of a buck-boost converter connected to a fuel cell, by switching the converter using a few logical rules. The resulting control loop was then inserted in a cascade-control framework to control the armature current in a DC motor, by manipulating its input voltage.

Wang et al. [9] applied multivariable robust control strategies to a PEMFC system. Initially, they modeled the PEMFC as a two-input-two-output system, where the inputs are air and hydrogen flow rates and the outputs are cell voltage and current. By fixing the output resistance, they aimed to control the cell voltage output by regulating the air and hydrogen flow rates. An H_∞ multivariable robust controller was designed to provide robust performance and reduce the hydrogen consumption of this system.

Mo Zhijun et al. [10] applied a fuzzy control technique to a PEMFC, in order to maintain the output voltage through the gas pressure control, for any load applied to the PEMFC output terminals. Zhan Yuedong et al. [11] designed a fuzzy-PI controller to control the hydrogen and air/oxygen mass flows, but also auxiliary variables such as the temperature, pressure, humidity of the membrane, and proportion of stoichiometry. Sakhare et al. [12] designed a power condition unit for a Solid Oxide Fuel Cell (SOFC) by incorporating a fuzzy logic control strategy, which is also suitable for any type of fuel cells with slight alterations, whereas Schumacher et al. [13] proposed a scheme for the online control of multiple cell units, using the Takagi Sugeno Kang (TSK) type fuzzy logic approach.

Arce et al. [14] developed an explicit predictive control strategy for a stand-alone PEMFC. Golber and Lewin [15] presented an alternative model-based controller for the regulation of a PEMFC. The model accounts for spatial dependencies of voltage, current, material flows, and temperatures in the fuel-cell channel. Analysis of the process model showed that the effective gain of the process undergoes a sign change in the normal operating range of the fuel cell, indicating that it cannot be stabilized using a linear controller with integral action and, consequently, they developed a non-linear model predictive controller. Wang et al. [16] applied a data-driven predictive control approach in order to solve the control problem of a SOFC system, since it was previously shown that the control of SOFC is challenging, due to the slow response and strict operating constraints. An MPC strategy was developed by Vahidi et al. [17] for a hybrid PEMFC system with ultracapacitors as an auxiliary source of power. Jurado [18] developed an MPC method for SOFCs, by integrating in it fuzzy models. The MPC concept was also used by Vahidi et al. [19] to avoid fuel-cell oxygen starvation, prevent air compressor surge and choke, and match at the same time an arbitrary level of current demand. The control scheme was designed on a hybrid configuration, in which a bank of ultracapacitors supplements the polymer electrolyte membrane fuel cell during fast current transients.

In this paper, a new methodology is presented for the optimal control of a PEMFC system. A simulation model is used first to generate a database that contains the values of the key system variables: the FC current, the compressor motor voltage, the FC net power and the oxygen excess ratio. An advanced neural network model (NNM) methodology is then applied to obtain a non-linear model between the input and the output variables. The database is also used for validating the accuracy of the produced models.

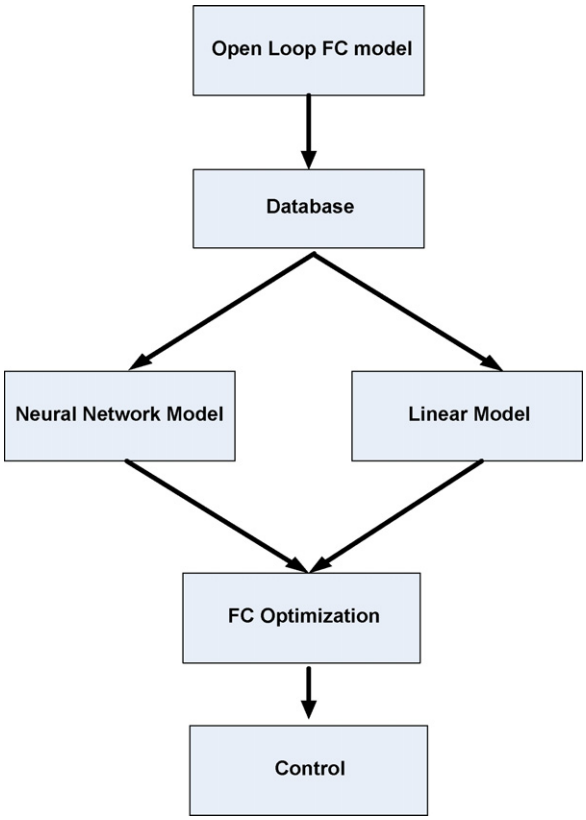

Fig. 1. Flowchart of the proposed PEMFC modeling, optimization and control procedure.

A Non-Linear Programming (NLP) optimization problem is formulated next, in order to obtain the optimal values of the decision variables. Eventually, a methodology based on the principles of MPC is designed, for the optimal control of the system response to successive sep-point changes of power demand. The optimal oxygen excess ratio value (determined by the solution of the optimization problem as described above) is used as an additional controlled variable. The efficiency of the produced MPC system is illustrated on a number of simulations, which show that a successful dynamic closed-loop behaviour can be achieved, while at the same time the consumption of hydrogen is minimized.

The proposed computational tool is summarized graphically in Fig. 1.

2. PEMFC modeling

2.1. Dynamic first-principle PEMFC model

The four-step methodology that is presented in this paper is built upon a detailed first-principle dynamic model of a PEMFC system, which has been proposed by Pukrushpan et al. [3]. The model contains both the main part (cell units) and auxiliary parts (compressor, cooling system, humidification system as well as the supply manifolds) of the PEMFC system. The overall inputs to the model are the stack current, I_{st}, and the compressor voltage, U_{cm}, whereas model outputs are the FC stack net power, P_{net}, and the oxygen excess ratio, λ_{O_2}, (input oxygen mass rate/oxygen reacted). More details about the development of the model, the complete set of differential and algebraic equations and the values of the model parameters are given in the above reference.

Table 1
Structure of the database used for the generation and validation of the meta-models.

No. of data	Input variables		Output variables	
	I_{st} (A)	U_{cm} (V)	P_{net} (W)	λ_{O_2}
1	60	50	14,580	1.312
2	100	65	21,640	1.176
3	150	90	29,750	1.235
...	...	...	...	...
...	...	...	...	...
...	75	60	17,600	1.369
...	...	...	...	...
524	...	...	...	...

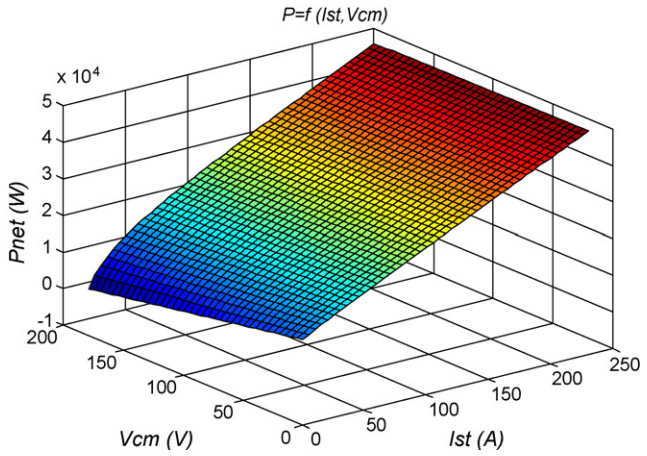

Fig. 2. FC stack net power as a function of stack current and compressor voltage.

2.2. Formulation of database

The available first-principle model was used to provide the steady-state output values corresponding to a number of input values that cover the full operational range of the system. In particular, values in the range (20 A–350 A) were assigned to stack current, whereas compressor voltage was set at values in the range (20 V–250 V). CPU time for each run was about 1 s on an Intel Core 2.2 GHz processor. The obtained results formed a database, which consists of 524 input-output examples. Table 1 presents the structure of the database and includes some indicative values of the input-output variables.

The contents of the database are presented graphically in Figs. 2 and 3. Fig. 2 presents in 3D view the net power as a function of stack current and compressor voltage, whereas Fig. 3 shows

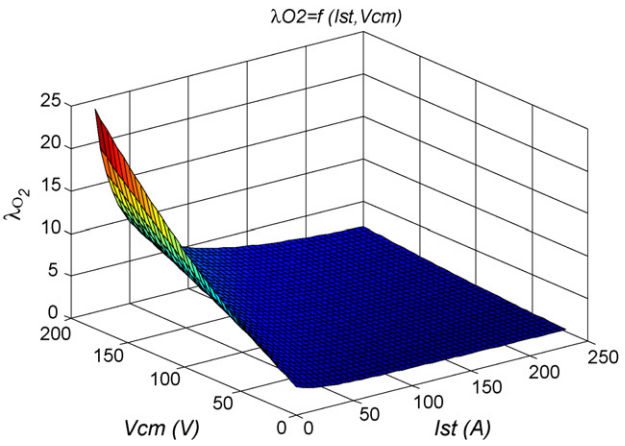

Fig. 3. Oxygen excess ratio as a function of stack current and compressor voltage.

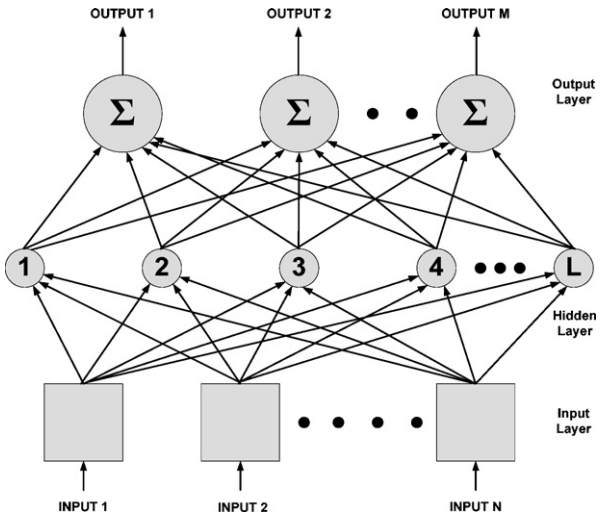

Fig. 4. Standard RBF neural network topology.

the oxygen excess ratio, as a function of the same input variables. It should be noted that in case we have access to experimental data obtained from a true fuel-cell system, these data can be stored in the database, instead of the first-principle model simulation results.

3. Development of meta-models

The database that was generated as described in the previous section was utilized for developing correlation equations between the output variables P_{net}, and λ_{O_2} and the input variables I_{st} and U_{cm} of the system. In particular, the Radial Basis Function (RBF) neural network architecture was adopted for producing the meta-models, due to its simple topology and the fast and robust algorithms that are available in the literature for training this type of networks. The topology of the RBF network is presented in Fig. 4 and consists of three layers: the input layer, the hidden layer and the output layer.

The input vector to the network $\mathbf{u}$ contains the input variables, i.e. $\mathbf{u} = [u_1, u_2]^T = [I_{st}, U_{cm}]^T$, while the neural network output vector provides the estimated values for the net power and oxygen excess ratio $\hat{\mathbf{y}} = [\hat{y}_1, \hat{y}_2]^T = \left[\hat{P}_{net}, \hat{\lambda}_{O_2}\right]^T$, which are calculated as weighted summations of the hidden node responses:

$$y_m = \sum_{j=1}^{L} w_{m,j} \cdot z_j(\mathbf{x}) \tag{1}$$

where

$$z_j(\mathbf{u}) = f(||\mathbf{u} - \mathbf{x}_j||_2^2) \tag{2}$$

In the above equations z_j is the response of the jth node, f is the Radial Basis Function, $\mathbf{x}_j$ is the centre of the jth node, L is the total number of hidden nodes and $w_{m,j}$ is the weight connecting the response of the jth node to the mth network output.

An RBF training procedure aims at the determination of the number of nodes in the hidden layer, the hidden node centres and the output weights, in order to minimize the deviation between the predicted and the measured values of the output variables over the set of the available data base. The training method used in this work is based on the fuzzy partition of the input space, which is produced by defining a number of triangular fuzzy sets in the domain of each input variable [20]. The centres of these fuzzy sets form a multidimensional grid on the input space. A rigorous selection algorithm chooses the most appropriate vertices on the grid, which are then used as the hidden node centres in the resulting RBF network model. The idea behind the selection algorithm is to place the centres in the multidimensional input space, so that the distance between any two centre locations is guaranteed to be greater than a lower limit, which is defined by the length of the edges on the grid. At the same time, the algorithm ensures that for any input example in the training set there is at least one selected hidden node that is close enough, according to an appropriately defined distance criterion. The so called "fuzzy-means" training method does not need the number of centres to be fixed before the execution of the method. Due to the fact that it is a one-pass algorithm, it is extremely fast, even in the case of a large database of input-output training data. One additional advantage is that the training algorithm used needs only one tuning parameter, namely the number of fuzzy sets that are utilized to partition each input dimension.

3.1. Correlation equations

The training procedure was used several times by altering each time the fuzzy partition of the input space (number of fuzzy sets defined in each input dimension), which is in fact the only design parameter that must be defined by the user, when utilizing the fuzzy-means algorithm. The average time needed to train an RBF network using an Intel Core 2.2 GHz processor was 18 s. The results were gradually improved up to the point where 16 fuzzy sets were used to partition the domain of each input variable, which corresponds to 57 hidden nodes. A further increase results to the overtraining phenomenon, where the performance of the produced model is not improved, although the model increases in size. The following statistics were used to measure the accuracy of the produced models:

Root Mean Squared Error

$$RMSE_m = \sqrt{\frac{SSE_m}{n-k-1}} = \sqrt{\frac{\sum_{i=1}^{n}(y_{m,i} - \widehat{y}_{m,i})^2}{n-k-1}} \tag{3}$$

Coefficient of Determination

$$R_m^2 = 1 - \frac{SSE_m}{SSY_m} = 1 - \frac{\sum_{i=1}^{n}(y_{m,i} - \hat{y}_{m,i})^2}{\sum_{i=1}^{n}(y_{m,i} - \bar{y}_m)^2} \tag{4}$$

$$F\text{-statistic}_m = \frac{(R_m^2/k)}{((1-R_m^2)/(n-k-1))} \tag{5}$$

where SSE_m measures the Sum of Squared Errors between the observations and the predicted values over the set of the available data for the mth output variable, while SSY_m measures the respective summation of squared deviations between the observations and their mean. In the above equations $y_{m,i}$ is the true value of the mth output variable for the ith observation, $\hat{y}_{m,i}$ is the associated model prediction, and $\bar{y}_m$ is the mean of all values of the mth output variable in the available data set. Finally, k is the number of the independent variables, and n the number of the available input-output data.

In order to test the reliability of the modeling methodology, the cross-validation method was used. Following this technique, a number of modified data sets is created by deleting in each case one or a small group (i.e. leave some out) of objects. For each data set, an input-output model is developed, by applying the modeling technique. Each model is evaluated, by measuring its accuracy in predicting the responses of the remaining data (the ones that have not been utilized in the development of the model). In particular, the Leave One-Out (LOO) cross-validation procedure was used in this study, which produces a number of models, by deleting each time one object from the training set. Obviously, the number of models produced by the LOO procedure is equal to the number of available examples n. Prediction Error Sum of Squares (*PRESS*) is

Table 2
Statistical indices corresponding to the produced RBF neural network model for both output variables.

	Statistical indices relating to RBF neural network model with 57 hidden nodes	
	P_{net}	λ_{O_2}
RMSE	52.9235	0.0426
R^2	0.9999	0.9997
F-Statistic	2,604,739.5	867,812.4
R^2_{CV}	0.9998	0.9996
S_{PRESS}	98.2385	0.0513

a standard index to measure the accuracy of a modeling method using the cross-validation technique. Based on the *PRESS* and *SSY* statistics, the R^2_{CV} and S_{PRESS} values can be easily calculated for each output variable. The formulae used to calculate all the aforementioned statistics are presented below:

$$R^2_{CV,m} = 1 - \frac{PRESS_m}{SSY_m} = 1 - \frac{\sum_{i=1}^{n}(y_{m,i} - \hat{y}^{LOO}_{m,i})^2}{\sum_{i=1}^{n}(y_{m,i} - \bar{y})^2} \quad (6)$$

$$S_{PRESS,m} = \sqrt{\frac{PRESS_m}{n-k-1}} \quad (7)$$

where $\hat{y}^{LOO}_{m,i}$ is the mth output variable prediction for observation i given by the model that has been trained using all the available data, except from observation i.

The statistical indices corresponding to the produced RBF neural network model for both output variables are summarized in Table 2.

Figs. 5 and 6 depict the true FC stack net power and oxygen excess ratio values, against the ones produced by the RBF neural network model, using the LOO cross-validation procedure. Good predictive abilities of both models are illustrated by noticing that in both cases all points lie very close to the main diagonal of the graph.

The RBF neural network modeling technique was further validated by developing models based on only 75% of the available data and evaluating them on the validation set, i.e. the rest of the database that was not used for the derivation of the model. In order to show that the success of one particular model is not due to a chance correlation, 100 random partitions of the data into training and validation sets (75 and 25% of the data, respectively) were performed to generate 100 different RBF models. The *RMSE* and R^2 statistics were calculated for each model using only the validation examples. Table 3 shows the min, max, mean and standard deviation of the *RMSE* and R^2 values obtained after performing the 100 runs.

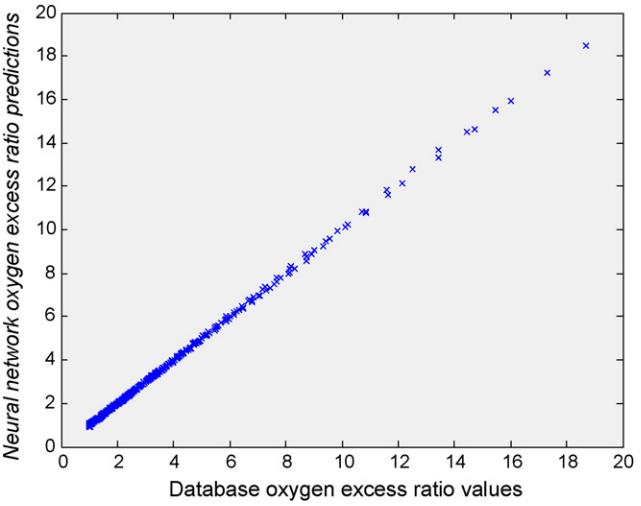

Fig. 6. Database oxygen excess ratio values against neural network predictions using the cross-validation procedure.

Table 3
Min, max, mean and standard deviation corresponding to *RMSE* and R^2 values obtained after performing 100 random partitions of the available data into training and validations sets.

Statistical indices	Min	Max	Mean	Standard deviation
RMSE (P_{net})	34.9082	233.4539	94.2287	38.2502
R^2 (P_{net})	0.9997	1	0.9999	0.0001
RMSE (λ_{O_2})	0.0259	0.1949	0.0602	0.0253
R^2 (λ_{O_2})	0.9972	0.9999	0.9995	0.0004

Fig. 7 presents the net power database values and the predictions of the neural network associated with the following statistics as far as the validation examples are concerned: *RMSE* = 108.49 and R^2 = 0.9999. Accordingly, Fig. 8 plots the oxygen excess ratio database values and the predictions of the neural network associated with the following statistics as far as the validation examples are concerned: *RMSE* = 0.0458 and R^2 = 0.9996. In both cases the difference between the two lines is almost invisible, thus illustrating the predictive ability of the produced models.

It must be mentioned here that before applying the RBF methodology, several models were developed using the linear regression

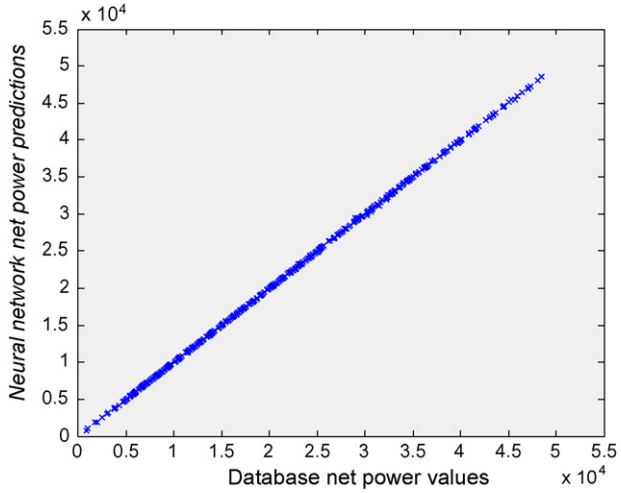

Fig. 5. Database net power values against neural network predictions using the cross-validation procedure.

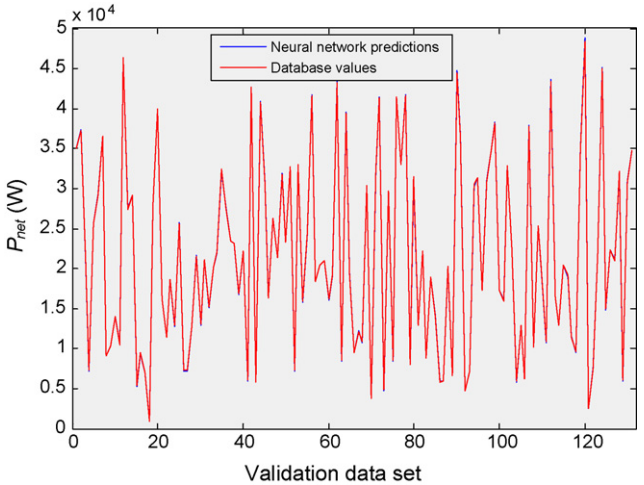

Fig. 7. Database net power values against neural network predictions for the validation data set.

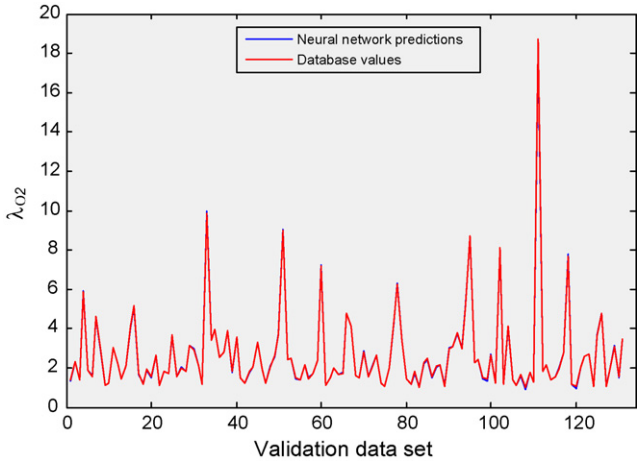

Fig. 8. Database oxygen excess ratio values against neural network predictions for the validation data set.

approach. The models were tested using the same validation routines that were used to test the RBF models. Best-fitting equations concerning the FC stack net power and the oxygen excess ratio are given below:

$$P_{net} = 159.15 I_{st} - 1198.59 \frac{U_{cm}}{I_{st}} + 7051.57 \quad (8)$$

$$\lambda_{O_2} = 0.0053 \frac{U_{cm}^2}{I_{st}} + 1.3187 \frac{U_{cm}}{I_{st}} + 0.1067 \quad (9)$$

The aforementioned equations are associated with the statistics shown in Table 4.

A comparison of the results included in Tables 3 and 4 clearly indicates that the RBF modeling methodology outperforms the linear regression approach, especially when prediction of net power is concerned. The RBF model will thus be used in the formulation of the optimization problem, which is described in the next section of the paper.

4. Optimization of the PEMFC performance

Performance of fuel-cell systems can be optimized by selecting appropriate stack current and compressor voltage input values [3]. These are not fixed, but depend on the power that is produced by the system. In this part of the paper, the meta-model produced in the previous section is utilized to compute the optimal values of the input variables for different levels of power demand. The optimization problem is formulated so that it takes into account the various constraints and limitations of the system. In Section 4.1 the formulation of the optimization problem is presented in detail.

Table 4
Statistical indices corresponding to the best models obtained using the linear regression technique.

	Statistical indices related to the best models obtained using the linear regression technique	
	P_{net}	λ_{O_2}
RMSE	2530.6	0.1282
R^2	0.9505	0.9975
F-Statistic	4992.5	103,740
R^2_{CV}	0.9496	0.9975
S_{PRESS}	2550	0.1299

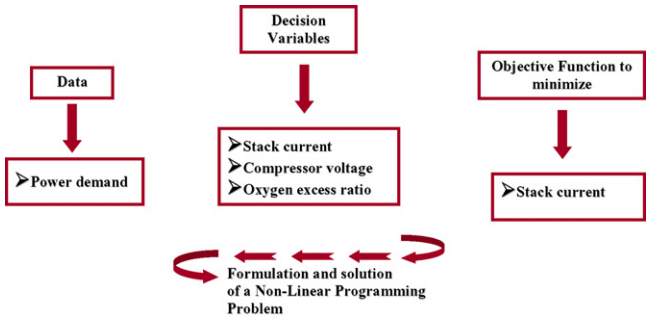

Fig. 9. Formulation of the Non-Linear Programming Problem.

4.1. Formulation of the optimization problem

The optimization problem is completely defined by the constraints that should be satisfied by the solution of the problem and the performance criterion, which is minimization of the FC stack current for a given load.

4.1.1. Constraints

i) The FC stack net power has been expressed as a function of I_{st}, U_{cm} using the RBF modeling methodology:

$$P_{net} = g_1(I_{st}, U_{cm}) \quad (10)$$

ii) Accordingly, an RBF model has been developed that expresses oxygen excess ratio as a function of I_{st}, U_{cm}:

$$\lambda_{O_2} = g_2(I_{st}, U_{cm}) \quad (11)$$

iii) FC stack net power should match the power demand by the consumer (set-point):

$$P_{net} = P_D \quad (12)$$

A number of additional constraints are used in the optimization problem to express physical limitations of the system and/or bound the system variables between desired upper and lower limits. In particular, the following upper and lower limits are imposed: net power (5 kW–45 kW), oxygen excess ratio (>1), stack current (20 A–350 A), compressor voltage (20 V–250 V).

4.1.2. Objective function

Selection of the objective function is a critical issue in the formulation of the optimization problem. Minimization of stack current I_{st} was selected as the performance criterion, because due to Faraday's First Law, stack current is proportional to the consumption of the costly fuel. Thus, by minimizing stack current, consumption of hydrogen is also reduced. Consequently, the optimization problem is formulated as follows:

$$\min_{I_{st}, U_{cm}, P_{net}, \lambda_{O_2}} I_{st} \quad (13)$$

Subject to the constraints (10)–(12) and the upper and lower bounds posed on the variables of the problem. The optimization problem is presented graphically in Fig. 9.

The previously described optimization problem is an NLP due to the non-linear neural network constraints (10) and (11). The global minimum of the problem was obtained using the GAMS modeling language [21]. The solution of the optimization problem contains the optimal values of all decision variables (optimal values for the manipulated variables stack current and compressor voltage, I^*_{st}, U^*_{cm}, as well as the optimal values for oxygen excess ratio, $\lambda^*_{O_2}$).

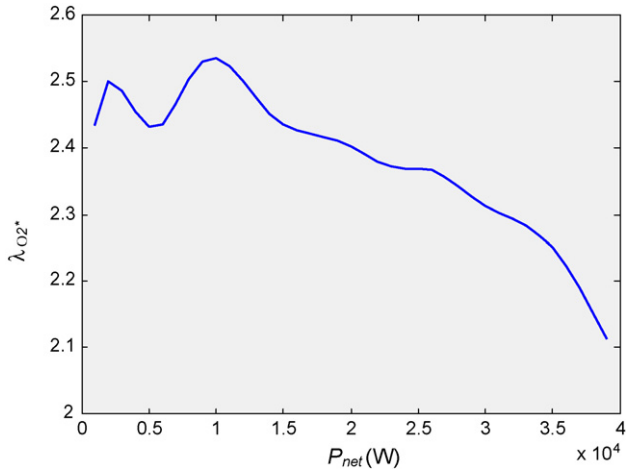

Fig. 10. Optimal $\lambda^*_{O_2}$-values as a function of power demand.

4.2. Solution of the optimization problem—results

The previously described optimization tool was used to obtain the optimal values of stack current, compressor voltage and oxygen excess ratio, corresponding to several levels of power demand, that cover the range of operation (5 kW–45 kW). The results are presented graphically in Figs. 10 and 11. In particular, Fig. 10 depicts the optimal values of the ratio $\lambda^*_{O_2}$ as a function of power demand, whereas Fig. 11 illustrates the optimal values of the input variables I^*_{st}, U^*_{cm}. These figures will prove useful when designing the process control strategies in the next section of this paper.

5. Control of the PEMFC

The final step in the development of the proposed framework is to design the optimal control strategy for the FC system. Control of fuel cells is a challenging problem, due to the multiple and contradicting criteria that define the performance of the system. The first priority in a fuel-cell control system is to respond both quickly and smoothly to power demand changes. This is particularly important for applications involving frequent changes of power demand, such as in automobile systems. However, changes in power demand cause sudden changes in the oxygen excess ratio values that are often responsible for the oxygen depletion phenomenon, which in turn can lead to membrane damage and to an abrupt FC system shut-down.

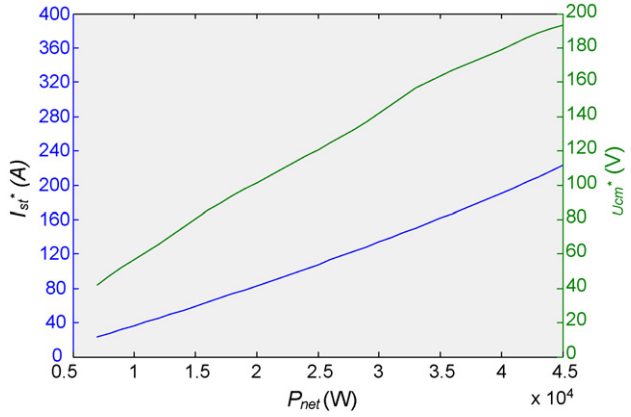

Fig. 11. Optimal values of input variables I^*_{st} and U^*_{cm} as functions of power demand.

The MPC methodology was chosen to design a control strategy which improves the dynamic behaviour of the system, while at the same time the fuel gas consumption is reduced. MPC has advanced to a popular control methodology for industrial and process applications mainly due to the inherent ability of the method to handle efficiently constraints and uncertainties in multivariable dynamical systems. Specifically, the dynamic matrix control (DMC) method was adopted (Cutler and Ramaker [22]), which requires simple step- (or pulse-) discrete-time response models, that can easily represent time delays and complex dynamics. Using the DMC methodology, at each sampling instance, the sequence of the manipulated variable values over a future control horizon is computed, by solving online an optimization problem which minimizes the offset (deviation of the controlled variables from the desired set-points) over a future prediction horizon, and the control energy over a future control horizon. The disturbance during the prediction horizon is assumed to be constant and equal to the difference between the process output and the model prediction at the current time instance.

5.1. Design of a DMC methodology

5.1.1. Development of finite impulse response (FIR) models

An FIR or convolution model is a discrete time filter that correlates dynamically an output variable of the system with an input variable, as follows:

$$y(t) = \sum_{i=1}^{C} h_i \cdot u(t-i) \tag{14}$$

where C is the number of past inputs used in the FIR model. The coefficients in the above model can be easily determined from the dynamic response of the output variable, after the introduction of a step or pulse change on the input variable, when the system is initially at steady state (Seborg et al. [23]). In case of a MIMO system, separate FIR models are developed for each pair of input-output variables. The FIR models can however be aggregated in a matrix form as follows:

$$\mathbf{y}(k) = \begin{bmatrix} y_1(k) \\ y_2(k) \\ \vdots \\ y_M(k) \end{bmatrix} = \sum_{i=1}^{C} H_i \cdot \mathbf{u}(t-i)$$

$$= \sum_{i=1}^{C} \begin{bmatrix} h_i^{1,1} & h_i^{1,2} & \dots & h_i^{1,N} \\ h_i^{2,1} & h_i^{2,2} & \dots & h_i^{2,N} \\ \vdots & \vdots & \vdots & \vdots \\ h_i^{M,1} & h_i^{M,2} & \dots & h_i^{M,N} \end{bmatrix} \begin{bmatrix} u_1(k-i) \\ u_2(k-i) \\ \vdots \\ u_N(k-i) \end{bmatrix} \tag{15}$$

where $h_i^{m,n}$ is the ith coefficient in the FIR model correlating the mth output variable with the nth input variable.

The fuel-cell system of the present study is a 2×2 MIMO system. The FIR models were produced by applying step changes on the manipulated variables (I_{st}, U_{cm}) when the system was initially at steady state, corresponding to I_{st} =100 A, U_{cm} =99 V (the respective steady-state output values are P_{net} = 23,255 W, $\lambda_{O_2} = 2$). The sampling time was set to 0.075 s, so that the FIR model captures the dynamic characteristics of the system, but at the same time uses a reasonable number of past input values (C = 30).

5.1.2. The DMC algorithm

In the DMC methodology, at time instance k a set of future manipulated variables (sequence of manipulated variable values over the control horizon) is selected, in order to minimize an appropriate objective function. The objective function includes both the deviations of the predicted controlled variables from their set-

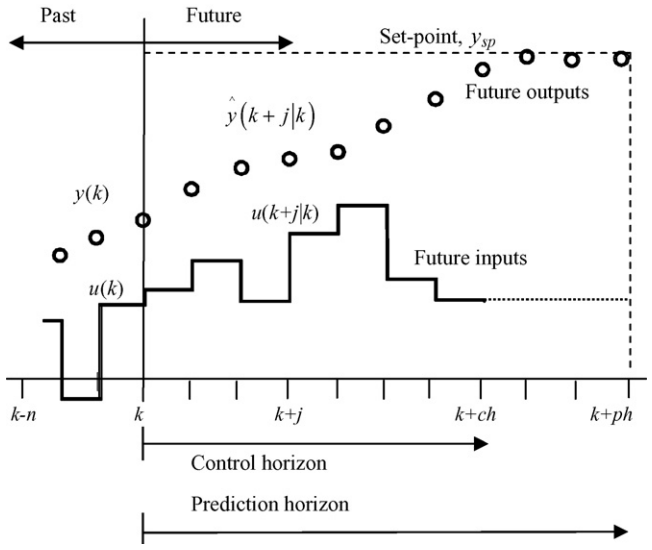

Fig. 12. DMC basic concept.

points over the future prediction horizon (ph), and the control effort over the control horizon (ch). Then, only the first control move is implemented and the optimization problem is formulated and solved again at the next time step $k+1$. Fig. 12 presents a schematic representation of the DMC philosophy.

In the sequel, the optimization problem that is solved at each time instance is presented in detail. It consists of the objective function, (Eq. (16)) which describes both the aforementioned control targets and a number of constraints, (Eqs. (17)–(21)):

Objective function:

$$\min_{\Delta\mathbf{u}(k),\Delta\mathbf{u}(k+1),\ldots,\Delta\mathbf{u}(k+ch)} \left(\sum_{i=1}^{ph} ||\mathbf{W}(\hat{\mathbf{y}}(k+i|k) - \mathbf{y}_{sp}(k))||_2^2 + \sum_{i=0}^{ch} ||\mathbf{R}\Delta\mathbf{u}(k+i)||_2^2 \right) \quad (16)$$

subject to:

$$\hat{\mathbf{y}}(k+i|k) = \left(\sum_{i=1}^{C} \mathbf{H}_i \cdot \mathbf{u}(k+i-1) \right) + \mathbf{d}(k), \quad i = 1, \ldots, ph \quad (17)$$

$$\mathbf{d}(k) = \mathbf{y}(k) - \hat{\mathbf{y}}(k|k) \quad i = 1, \ldots, ph \quad (18)$$

$$\Delta\mathbf{u}(k+i) = \mathbf{u}(k+i) - \mathbf{u}(k+i-1) \quad i = 1, \ldots, ch \quad (19)$$

$$\mathbf{u}_{\min} \le \mathbf{u}(k+i) \le \mathbf{u}_{\max} \quad i = 1, \ldots, ch \quad (20)$$

$$\Delta\mathbf{u}(k+i) = 0 \quad i = ch+1, \ldots, ph \quad (21)$$

In the above formulation of the optimization problem, $\hat{\mathbf{y}}(k+i|k)$ is the i-step (ahead) prediction of the controlled-variable vector, $\mathbf{y}_{sp}(k)$ is a vector containing the current set-point values of the controlled variables, $\Delta\mathbf{u}(k+i)$ are the future control moves, $\mathbf{R}$, $\mathbf{W}$ are diagonal square weight matrices, and $\mathbf{d}(k)$ is a correction term, calculated as the current (at time instance k) difference between the true output vector and the respective model prediction (Eq. (18)). It should be noted that although the FIR model is able to predict the future dynamic behaviour of the fuel-cell system (Eq. (17)), it is assumed that the future set-point changes and disturbances are completely unknown. The set-point vector is thus set to its current value $\mathbf{y}_{sp}(k)$ throughout the entire prediction horizon and the same happens with the correction term $\mathbf{d}(k)$. Eq. (19) computes the control move at each time instance $k+i$, as the difference between the input vector at the same time instance and the input vector in the previous time instance. Eq. (20) contains hard constraints that bound the manipulated variables between upper ($\mathbf{u}_{\max}$) and lower ($\mathbf{u}_{\min}$) values due to physical limitations. Eq. (21) ensures that no control moves are allowed after the end of the control horizon.

5.2. Implementation of the DMC controller on the PEMFC system

The DMC control strategy combined with the operational optimization results presented in the previous section are integrated in this section, in order to achieve a satisfactory dynamic performance, while at the same time fuel consumption is minimized. The proposed methodology is implemented as follows.

At each time instance the set-point for the two controlled variables are defined. The set-point for net power demand is determined by the current energy needs of the user of the fuel-cell system. The frequency of set-point changes in energy demand depends on the particular fuel-cell application. It is most probable, that set-point changes will be more frequent for a vehicle fuel-cell system, compared to a stationary fuel-cell application. As mentioned in the formulation of the optimization problem in the previous subsection, the control methodology does not assume any knowledge about future set-point changes. The set-point for the second controlled variable (oxygen excess ratio) is then automatically determined by the results presented in Section 4. In particular, the function corresponding to Fig. 10 is used to obtain the oxygen excess ratio value that minimizes fuel gas consumption. Then, the optimization problem defined by Eqs. (16)–(21) is solved to obtain the optimal sequence of manipulated variables. In the present simulations, the prediction and control horizons were set to $ph = 50$ and $ch = 40$, respectively. From the optimal sequence of manipulated variables, only the first element is actually applied to the system, for a time interval equal to the sampling period that was used to obtain the FIR model coefficients. At the end of this period the entire procedure is repeated.

The proposed methodology was tested on the scenario presented in Table 5 which involves a number of step changes on the power demand set-point. As mentioned in the beginning of the section, the two performance criteria (satisfactory dynamic response of both controlled variables, P_{net}, λ_{O_2}) are contradictory. It will be shown that by tuning appropriately the weight matrices in Eq. (16), special emphasis can be given on one over the other performance criterion. In particular:

Case I: The weight matrices are $\mathbf{W} = \begin{bmatrix} 0.003 & 0 \\ 0 & 100 \end{bmatrix}$, $\mathbf{R} = \begin{bmatrix} 0.01 & 0 \\ 0 & 1/1.3 \end{bmatrix}$ and the responses of the controlled variables are shown in Figs. 13 and 14.

Case II: The weight matrices are $\mathbf{W} = \begin{bmatrix} 100 & 0 \\ 0 & 10 \end{bmatrix}$, $\mathbf{R} = \begin{bmatrix} 0.01 & 0 \\ 0 & 1/1.3 \end{bmatrix}$ and the responses of the controlled variables are shown in Figs. 15 and 16.

Table 5
A testing scenario for the control methodologies consisting of several net power set-point step tests.

Time instance (s)	Net power, P_{net} (W)	λ_{O_2}
0	8,350	2.496
3	12,540	2.452
6	16,730	2.527
9	35,360	2.323
12	18,500	2.488
15	12,350	2.447

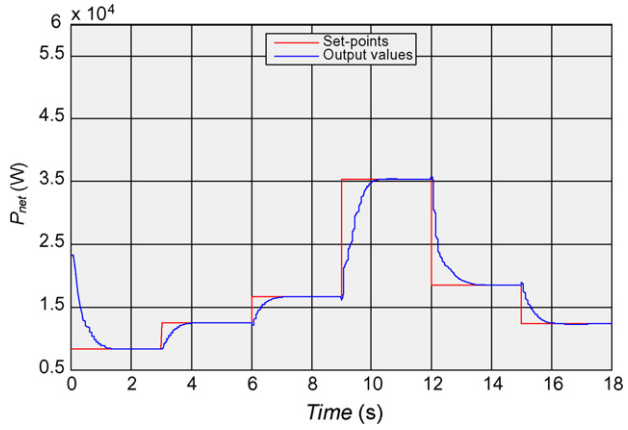

Fig. 13. Response of net power (DMC, Case I).

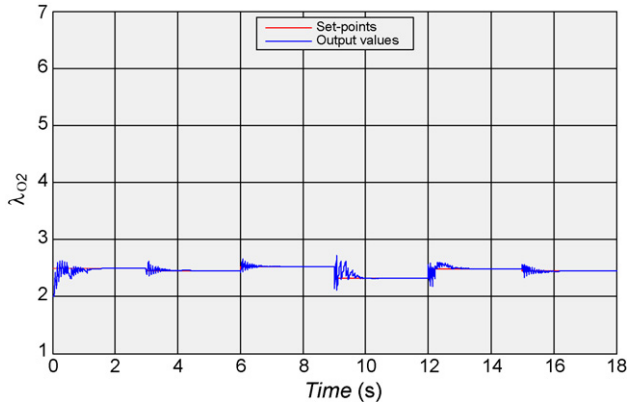

Fig. 14. Response of oxygen excess ratio (DMC, Case I).

The efficiency of the method is illustrated by observing that the control strategy is satisfactory in both cases, because both controlled variables respond quickly and the system reaches the desired set-points with no-offset. However, the DMC tuning of Case I clearly favours the dynamic response of oxygen excess ratio, which is driven to the desired set-point after some oscillations of very low amplitude, whereas 1 s is needed for the net power to reach the desired set-point. On the contrary, using the tuning strategy of Case II, sharp peaks are observed as far as the dynamic response of oxygen excess ratio is concerned, but at the same time the dynamic behaviour of net power is improved (almost instant responses to set-point changes). However, there is one exception which is the net power response when the set-point is set to its highest value.

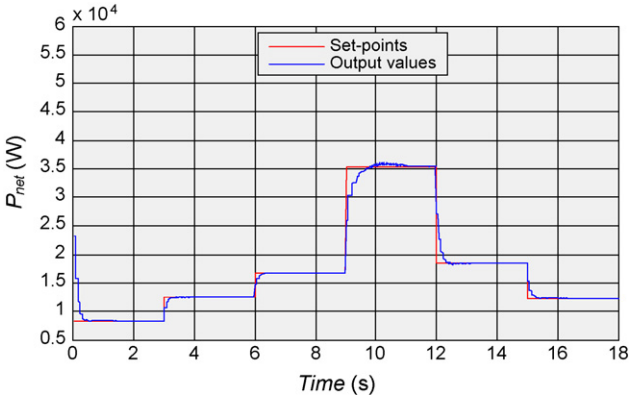

Fig. 15. Response of net power (DMC, Case II).

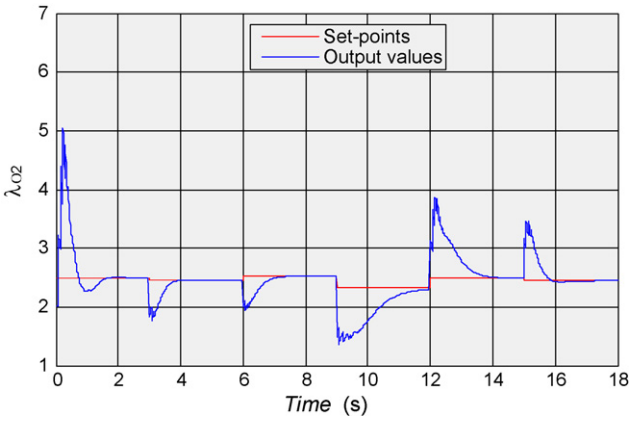

Fig. 16. Response of oxygen excess ratio (DMC, Case II).

For this particular set-point step change, the net power response is as slow as in Case I. This is due to the modeling error which becomes significant when the system operates in a region which is not close to the operating range that was used for obtaining the FIR models.

5.3. Design of a feedforward control scheme

For comparison purposes, a feedforward controller was also designed based on the results of Section 4. In particular, the information contained in Fig. 11 was used to develop look-up tables, from which the optimal values of the manipulated variables are calculated, as functions of the net power demand. The feedforward controller was applied on the same sequence of net power set-point changes that was used to test the DMC methodology (Table 5). The responses of the controlled variables are depicted in Figs. 17 and 18. It is clear that the feedforward controller is not able to achieve zero offset. This is due to the fact that, contrary to the DMC methodology, the feedforward controller lacks integral action. Additionally, the dynamic behaviour of λ_{O_2} contains sharp and intense changes. These may cause the abrupt shut-down of the system in a real application. They also pose dynamic stress onto the FC membranes due to pressure oscillations and possible oxygen starvation [19,24], which reduces lifetime of the membranes.

5.4. Testing the robustness of the control strategies

In this subsection, robustness of the proposed MPC methodology is tested on a typical defection case, that happens during the operation of fuel-cell systems. In particular, it is assumed that 21 of the 381 cell units that constitute the FC stack are out of operation, due to membrane cracking. The DMC methodology tuned with

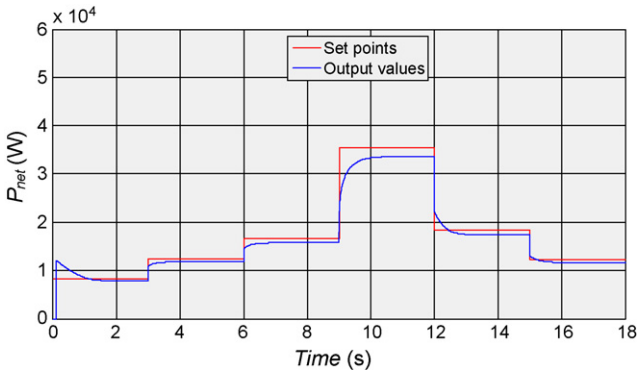

Fig. 17. Response of net power (feedforward controller).

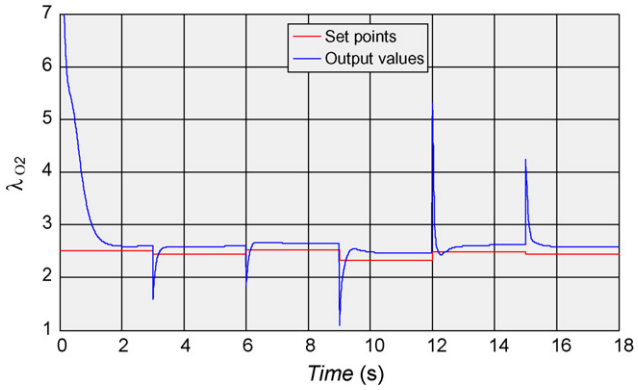

Fig. 18. Response of oxygen excess ratio (feedforward controller).

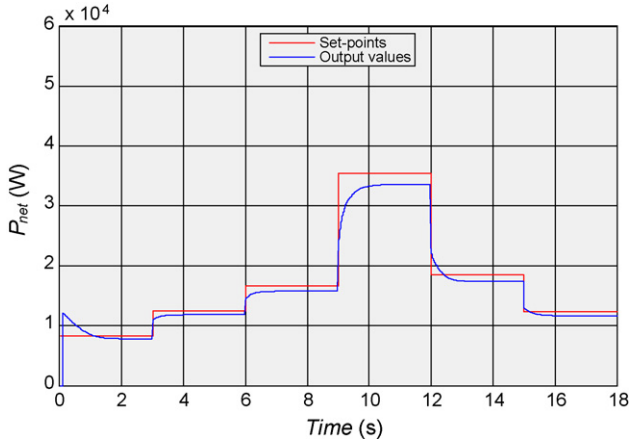

Fig. 19. Response of net power in robustness test (feedforward controller).

the Case I strategy and the feedforward controller were tested on the disturbed system and the responses concerning the controlled variables are shown in Figs. 19–22. Robustness of the proposed method is illustrated by noticing that no significant modifications are observed in the dynamic responses of the controlled variables, compared to the case where all cell unit operate normally (Figs. 13 and 14), and, the method still produces zero steady-state effort. The dynamic behaviour of the feedforward controller is similar to the one presented in Figs. 17 and 18, but the steady state offset is further increased.

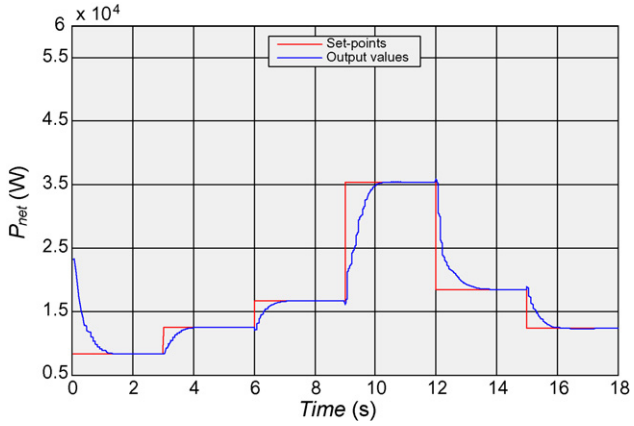

Fig. 20. Response of net power in robustness test (DMC, Case I).

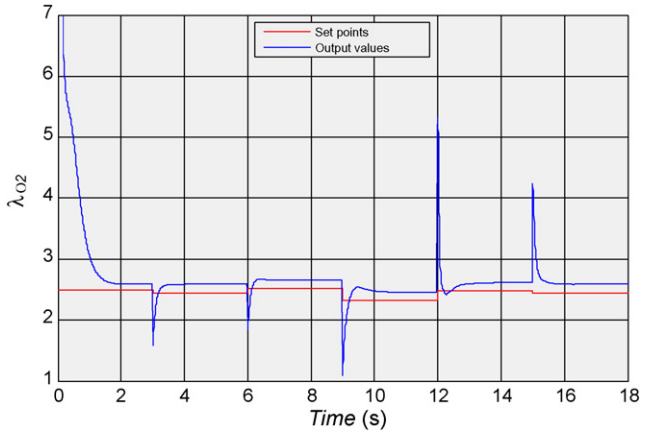

Fig. 21. Response of oxygen excess ratio in robustness test (feedforward controller).

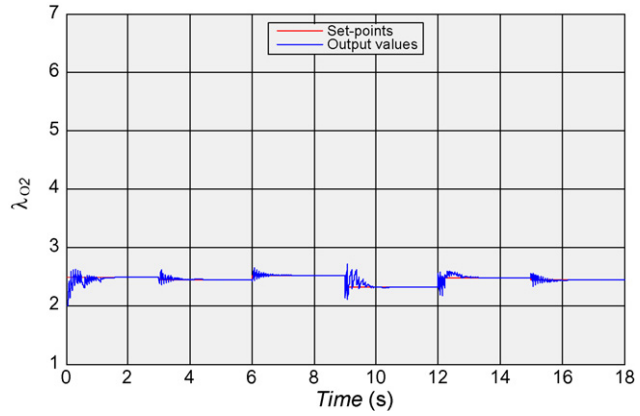

Fig. 22. Response of oxygen excess ratio in robustness test (DMC, Case I).

6. Conclusions

In this work a computational tool for the optimal control of FC systems was developed by integrating and combining a number of modeling, optimization and control technologies. The produced methodology is built upon four steps that may be summarized as follows:

- First, via a simulation model, a database is generated which includes values of the input variables (stack current, I_{st}, compressor voltage, U_{cm}) and the corresponding values of output variables (net output power, P_{net}, ratio of incoming oxygen mass flow to the oxygen that reacts, λ_{O_2});
- Second step is the development of mathematical relationships between the input and output variables. In particular, the RBF neural network architecture was utilized for producing the input-output "meta-models";
- In the third step, an NLP optimization problem was formulated that takes into account the constraints and limitations of the system. The objective function to be minimized is stack current for a given value of power demand. Based on the formulation and solution of the NLP problem, a look-up table is developed, containing the optimal values of the system variables, for any possible value of power demand in the operating range of the system;
- Finally, a methodology based on the principles of MPC is designed for the optimal control of the system response to successive sep-point changes of power demand. The optimal λ_{O_2}-value (determined by the solution of the optimization problem as described above) is used as an additional control variable. The

efficiency of the produced MPC system is illustrated in a number of simulations, which show that a successful dynamic closed-loop behaviour can be achieved, while at the same time the consumption of hydrogen is minimized. It is illustrated that by appropriate tuning, the proposed control strategy can produce zero steady-state offset, without the risk of oxygen depletion (oxygen excess ratio does not fall below the value of 1.8 which is, in fact, much higher than the safety limit of 1.5 [3]).

References

[1] R.N. Methekar, V. Prasad, R.D. Gudi, J. Power Sources 165 (2007) 152–170.
[2] C.H. Woo, J.B. Benziger, Chem. Eng. Sci. 62 (2007) 957–968.
[3] J.T. Pukrushpan, A.G. Stefanopoulou, H. Peng, Control of Fuel Cell Power Systems, Springer, New York, 2004.
[4] L. Guidong, Y. Wensheng, T. Zhishou, Proc. ISDA 2006: Sixth Int. Conf. on Intelligent Systems Design and Applications, vol. 1, 2006, pp. 1104–1110.
[5] P. Rodatz, G. Paganelli, L. Guzzella, Proc. Am. Control Conf., vol. 3, 2003, pp. 2043–2048.
[6] A. Di Domenico, A. Miotti, M. Alhetairshi, Y.G. Guezennec, S.S.V. Rajagopalan, S. Yurkovich, Proc. Am. Control Conf., 2006, pp. 478–483.
[7] M.A. Danzer, J. Wilhelm, H. Aschemann, E.P. Hofer, J. Power Sources 176 (2008) 515–522.
[8] F. Zenith, S. Skogestad, J. Process Control 17 (2007) 333–347.
[9] F.C. Wang, H.T. Chen, Y.P. Yang, J.Y. Yen, J. Power Sources 177 (2008)393–403.
[10] M. Zhijun, Z. Xinjian, C. Guangyi, Proc. IEEE Int. Conf. on Ind. Techn., 2005, pp. 220–224.
[11] Z. Yuedong, Z. Jianguo, G. Youguang, J. Jianxun, Proc. of the 26th Chinese Control Conference, 2007, pp. 345–349.
[12] A. Sakhare, A. Davari, A. Feliachi, J. Power Sources 135 (2004) 165–176.
[13] J.O. Schumacher, P. Gemmar, M. Denne, M. Zedda, M. Stueber, J. Power Sources 129 (2004) 143–151.
[14] A. Arce, D.R. Ramiĩrez, A.J. Del Real, C. Bordons, Proc. IEEE Conf. on Decision and Control, 2008, pp. 6088–6093.
[15] J. Golbert, D.A. Lewin, J. Power Sources 135 (2004) 135–151.
[16] X. Wang, B. Huang, T. Chen, J. Process Control 17 (2006) 103–114.
[17] A. Vahidi, A. Stefanopoulou, H. Peng, IEEE Trans. Control Syst. Technol. 14 (2006) 1047–1057.
[18] F. Jurado, J. Power Sources 158 (2008) 245–253.
[19] A. Vahidi, A. Stefanopoulou, H. Peng, Proc. of the 2004 Amer. Control Conf., Boston, MA, 2004, pp. 834–839.
[20] H. Sarimveis, A. Alexandridis, G. Tsekouras, G. Bafas, Ind. Eng. Chem. Res. 41 (2002) 751–759.
[21] A. Brooke, D. Kendrick, A. Meeraus, R. Raman, GAMS, User Guide. Available with the GAMS system or from http://www.gams.com, 1998.
[22] C.R. Cutler, B.C. Ramaker, Paper WP5-B, AIChE National Meeting, Houston, USA, 1980.
[23] D.E. Seborg, T.F. Edgar, D.A. Mellichamp, Process Dynamics and Control, Wiley & Sons, New York, 2004.
[24] T. Bocklisch, Sc. Wo, St. Bo, Proc. 4th European PV-Hybrid and Mini-Grid Conference, Athens, 2008.